

Low-energy p - d scattering and ${}^3\text{He}$ in pionless EFT

Sebastian König* and H.-W. Hammer†

*Helmholtz-Institut für Strahlen- und Kernphysik (Theorie)
and Bethe Center for Theoretical Physics,
Universität Bonn, 53115 Bonn, Germany*

(Dated: March 11, 2022)

Abstract

We calculate low-energy proton–deuteron scattering in the framework of pionless effective field theory. In the quartet channel, we calculate the elastic scattering phase shift up to next-to-next-to-leading order in the power counting. In the doublet channel, we perform a next-to-leading order calculation. We obtain good agreement with the available phase shift analyses down to the scattering threshold. The phase shifts in the region of non-perturbative Coulomb interactions are calculated by using an optimised integration mesh. Moreover, the Coulomb contribution to the ${}^3\text{He}$ - ${}^3\text{H}$ binding energy difference is evaluated in first order perturbation theory. We comment on the implications of our results for the power counting of subleading three-body forces.

arXiv:1101.5939v3 [nucl-th] 11 Oct 2011

*Electronic address: koenig@hiskp.uni-bonn.de

†Electronic address: hammer@hiskp.uni-bonn.de

I. INTRODUCTION

Although Quantum Chromodynamics (QCD) is widely accepted as the underlying theory of strong interactions, *ab initio* calculations of nuclear properties in Lattice QCD remain a large theoretical challenge [1]. In nuclear physics, the relevant degrees of freedom are pions and nucleons, and much of the computational effort in such a calculation would be required for generating the correct degrees of freedom from quarks and gluons rather than their interactions. Traditionally, nucleon–nucleon interactions are described via phenomenological nuclear forces fitted to scattering data. Effective field theory (EFT) provides a powerful method to construct nuclear forces with a direct connection to QCD in a systematic, model-independent way [2–4].

For very low energies and momenta $p \lesssim M_\pi$, the non-analyticities from pion exchange cannot be resolved and one can hence use an EFT including only short-range contact interactions between nucleons [5, 6]. This theory is constructed to reproduce the effective range expansion [7] in the two-body system and recovers Efimov’s universal approach to the three-nucleon problem [8, 9]. An advantage of the EFT formulation is that it can be extended to higher-body systems and external currents in a straightforward way.

The extension of this EFT to include the long-range Coulomb interaction was first discussed by Kong and Ravndal for the proton–proton channel [10, 11]. In Ref. [12], this analysis was extended to next-to-next-to-leading order. A renormalisation group analysis of proton–proton scattering in a distorted wave basis was carried out in Refs. [13, 14]. Moreover, this theory was applied to proton–proton fusion in Refs. [15, 16]. An extension of this formalism to three charged particles would be important for the possible interpretation of the Hoyle state in ^{12}C as an Efimov state of α particles [17] and the cluster EFT for halo nuclei [18].

In this work, we are interested in the simpler problem of a three-body system with two charged particles. Close to threshold, the Coulomb interaction is strong. Its long-range nature requires special care in the non-perturbative treatment using momentum space integral equations. At higher energies, the Coulomb interaction becomes perturbative. Rupak and Kong have formulated a power counting for the Coulomb contributions in the quartet channel of proton–deuteron (p – d) scattering. They calculated the phase shifts to next-to-next-to-leading order (N^2LO) in the pionless EFT and included Coulomb effects to next-to-leading order (NLO) [19]. However, they were not able to extend their calculation to the threshold region below center-of-mass momenta of 20 MeV. They did not consider the doublet channel and the ^3He bound state. A leading order calculation of the ^3He nucleus including non-perturbative Coulomb interactions was recently presented by Ando and Birse [20]. Including isospin breaking effects in the nucleon–nucleon scattering lengths, they obtain a surprisingly accurate description of the ^3He – ^3H binding energy difference but they did not consider scattering observables. A similar study to NLO in the pionless EFT was carried out using the resonating group method [21]. Their results do not include isospin breaking and are consistent with other determinations of the ^3He – ^3H binding energy difference.

In this paper, we focus on p – d scattering observables in the quartet and doublet channels. We extend the power counting by Rupak and Kong for the Coulomb contribution to the doublet channel. By using a special integration mesh, we are able to calculate the phase shifts in both channels down to momenta of order 3 MeV. We also provide a perturbative evaluation of the Coulomb contribution to the ^3He – ^3H binding energy difference.

II. FORMALISM

In this section, we briefly summarise the formalism required for calculating p - d scattering in the pionless theory. More technical details can, *e.g.*, be found in Refs. [19, 22–25].

A. Effective Lagrangian

We use the effective Lagrangian

$$\begin{aligned} \mathcal{L} = & N^\dagger \left(iD_0 + \frac{\mathbf{D}^2}{2M_N} \right) N - d^{i\dagger} \left[\sigma_d + \left(iD_0 + \frac{\mathbf{D}^2}{4M_N} \right) \right] d^i - t^{A\dagger} \left[\sigma_t + \left(iD_0 + \frac{\mathbf{D}^2}{4M_N} \right) \right] t^A \\ & + y_d [d^{i\dagger} (N^T P_d^i N) + \text{h.c.}] + y_t [t^{A\dagger} (N^T P_t^A N) + \text{h.c.}] + \mathcal{L}_{\text{photon}} + \mathcal{L}_3, \end{aligned} \quad (1)$$

with the nucleon field N and two dibaryon fields d^i (with spin 1 and isospin 0) and t^A (with spin 0 and isospin 1), corresponding to the deuteron and the spin-singlet virtual bound state in S-wave nucleon–nucleon scattering. Both dibaryon fields are formally ghosts since their kinetic terms have a negative sign. This is required to avoid the Wigner bound and reproduce the positive value of the effective range with short-range interactions [26]. Spin and isospin degrees of freedom are included by treating the field N as a doublet in both spaces, but for notational convenience we have suppressed the spin and isospin indices of N . The projection operators,

$$P_d^i = \frac{1}{\sqrt{8}} \sigma^2 \sigma^i \tau^2, \quad P_t^A = \frac{1}{\sqrt{8}} \sigma^2 \tau^2 \tau^A, \quad (2)$$

with $\vec{\sigma}$ ($\vec{\tau}$) operating in spin (isospin) space, project out the 3S_1 and 1S_0 nucleon–nucleon partial waves, respectively.

The covariant derivative

$$D_\mu = \partial_\mu + ieA_\mu \cdot \hat{Q}, \quad (3)$$

where \hat{Q} is the charge operator, includes the coupling to the electromagnetic field. Furthermore, we have the kinetic and gauge fixing terms for the photons,

$$\mathcal{L}_{\text{photon}} = -\frac{1}{4} F_{\mu\nu} F^{\mu\nu} - \frac{1}{2\xi} (\partial_\mu A^\mu - \eta_\mu \eta_\nu \partial^\nu A^\mu)^2, \quad (4)$$

of which we only keep contributions from Coulomb photons. These correspond to a static Coulomb potential between charged particles, but for convenience we introduce Feynman rules for a Coulomb photon propagator,

$$i\Delta_{\text{Coulomb}}(k) = \frac{i}{\mathbf{k}^2 + \lambda^2}, \quad (5)$$

which we draw as a wavy line, and factors $(\pm ie \cdot \hat{Q})$ for the vertices.¹ Following [19], we have introduced a small photon mass λ to regulate the singularity of the propagator at zero

¹ Due to the sign convention chosen in the Lagrangian (1), dibaryon–photon vertices get an additional minus sign.

momentum transfer. As we will discuss later on, this regulator will be removed by numerical extrapolation back to vanishing photon mass.

In the doublet-channel of the three-nucleon system, a three-body contact interaction is required for renormalisation at leading order [22]. It can be written as

$$\mathcal{L}_3 = -M_N \frac{H(\Lambda)}{\Lambda^2} \left(y_d^2 N^\dagger (\vec{d} \cdot \vec{\sigma})^\dagger (\vec{d} \cdot \vec{\sigma}) N + y_t^2 N^\dagger (\vec{t} \cdot \vec{\tau})^\dagger (\vec{t} \cdot \vec{\tau}) N + \frac{1}{3} y_d y_t \left[N^\dagger (\vec{d} \cdot \vec{\sigma})^\dagger (\vec{t} \cdot \vec{\tau}) N + \text{h.c.} \right] \right), \quad (6)$$

where Λ is a momentum cutoff applied in the three-body equations discussed below and $H(\Lambda)$ a known log-periodic function of the cutoff that depends on a three-body parameter Λ_* .

B. Dibaryon propagators

In the strong sector, we adopt the standard power counting for large S-wave scattering length [5, 6]. A nucleon bubble together with a bare dibaryon propagator scales as $\mathcal{O}(1)$. The bare dibaryon propagators therefore are dressed by nucleon bubbles to all orders. The resulting geometric series for the full propagators are shown in Fig. 1.

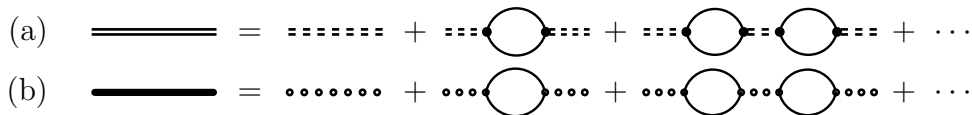


FIG. 1: Full dibaryon propagators in (a) the 3S_1 state (*i.e.* the deuteron) and (b) the 1S_0 state.

For convenience, we also resum the effective range corrections. If desired, the perturbative expressions can always be obtained by re-expanding the propagators. We do not go into the details of the calculations here and simply quote the results for the renormalised propagators, which we obtain by demanding that the effective range expansions

$$k \cot \delta_d = -\gamma_d + \frac{\rho_d}{2}(k^2 + \gamma_d^2) + \dots \quad (7)$$

around the deuteron pole, and

$$k \cot \delta_t = -\frac{1}{a_t} + \frac{\rho_t}{2}k^2 + \dots \quad (8)$$

for the singlet channel are reproduced. In writing Eq. (8) we have used that $\rho_t = r_{0t}$ to the order we are working. This yields the expressions

$$i\Delta_d^{ij}(p) = -\frac{4\pi i}{M_N y_d^2} \cdot \frac{\delta^{ij}}{-\gamma_d + \sqrt{\frac{\mathbf{p}^2}{4} - M_N p_0 - i\varepsilon - \frac{\rho_d}{2} \left(\frac{\mathbf{p}^2}{4} - M_N p_0 - \gamma_d^2 \right)}}, \quad (9)$$

and analogously

$$i\Delta_t^{AB}(p) = -\frac{4\pi i}{M_N y_t^2} \cdot \frac{\delta^{AB}}{-\frac{1}{a_t} + \sqrt{\frac{\mathbf{p}^2}{4} - M_N p_0 - i\varepsilon} - \frac{\rho_t}{2} \left(\frac{\mathbf{p}^2}{4} - M_N p_0 \right)} \quad (10)$$

for the spin-singlet dibaryon. These expressions are valid to N²LO. At leading order, effective range corrections are not included and the dibaryon kinetic terms do not contribute. The corresponding propagators are obtained by setting $\rho_t = 0$ and $\rho_d = 0$ in Eqs. (9) and (10).

The deuteron wave function renormalisation constant is given as the residue at the bound state pole:

$$Z_0^{-1} = i \frac{\partial}{\partial p_0} \frac{1}{i\Delta_d(p)} \Big|_{p_0 = -\frac{\gamma_d^2}{M_N}, \mathbf{p}=0} \quad (11)$$

C. Coulomb contributions in the proton–proton system

The Coulomb interaction breaks the isospin symmetry that is implicit in the dibaryon propagators from the previous subsection. For the pp -part of the singlet dibaryon we can also have Coulomb photon exchanges inside the nucleon bubble. These can be resummed to all orders, yielding a dressed nucleon bubble [10, 11], which is then used to calculate the full singlet dibaryon propagator in the pp -channel, as shown in Fig. 2.

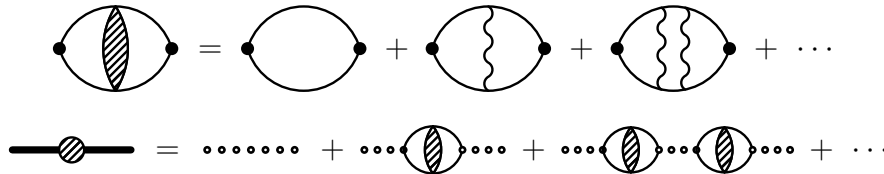


FIG. 2: Dressed nucleon bubble and full singlet dibaryon propagator in the pp -channel.

The result for the leading order propagator is [20]

$$i\Delta_{t,pp}^{AB}(p) = -\frac{4\pi i}{M_N y_t^2} \cdot \frac{\delta^{AB}}{-1/a_C - 2\kappa H(\kappa/p')} \quad , \quad \kappa = \frac{\alpha M_N}{2} \quad (12)$$

with

$$p' = i\sqrt{\mathbf{p}^2/4 - M_N p_0 - i\varepsilon} \quad (13)$$

and

$$H(\eta) = \psi(i\eta) + \frac{1}{2i\eta} - \log(i\eta) \quad (14)$$

where ψ denotes the logarithmic derivative of the Γ -function. Effective range corrections can be included in the same way as described above.

D. Power counting

The power counting of pionless effective field theory has been extensively discussed in the literature (see the reviews [2–4] and references therein). We will thus be rather brief on this subject here. We will, however, elaborate a bit on the power counting for the Coulomb sector of the theory, as it was introduced in [19].

1. Strong sector

The low-energy scale Q of the theory is set by the deuteron binding momentum $\gamma_d \sim 45$ MeV. We can formally count the external momenta k, p to be of the same order. Since we are working in a theory without explicit pions, the natural ultraviolet cutoff of our theory is of the order of the pion mass, $\Lambda \sim M_\pi$. Which cutoff is best to use in practice depends on whether one discusses the quartet-channel system (where short-range effects are suppressed by the Pauli principle), or the doublet-channel system. In the first case one finds that already $\Lambda \approx 140$ MeV is sufficient for an accurate description, whereas in the latter case we have to set the cutoff to a few hundred MeV to reach convergence. The combination of the two scales yields the expansion parameter $\mathcal{O}(Q/\Lambda)$.

A further relevant scale in our system is the nucleon mass M_N . It appears explicitly in kinetic energies, which scale as $\mathcal{O}(Q^2/M_N)$. As a consequence, the nucleon propagator scales as $\mathcal{O}(M_N/Q^2)$ and the loop integration measure $d^3q dq_0$ scales as $\mathcal{O}(Q^5/M_N)$. We assume $y_d^2 \sim y_t^2 \sim \Lambda/M_N^2$ for the nucleon–dibaryon coupling constants and $\sigma_d \sim \sigma_t \sim Q\Lambda/M_N$ for the bare dibaryon propagator constants.

2. Including Coulomb photons

From the form of the Coulomb potential in momentum space,

$$V_c(q) \sim \frac{\alpha}{q^2}, \quad (15)$$

it is clear that Coulomb contributions are dominant for small momentum transfers. As noted in [19], they enter $\sim \alpha M_N/q$. This behaviour is not captured by the power counting for the strong sector. Hence, when one wants to perform calculations including Coulomb effects for small external momenta, one can no longer assume that all momenta scale with $Q \sim \gamma_d$. Instead, one has to keep track of the new scale introduced by the external momenta separately. We generically denote this scale by p and assume $p \ll Q$ for the power counting. As noted in [19], this means that we make a simultaneous expansion in *two* small parameters Q/Λ and $p/(\alpha M_N)$. For $p \gtrsim Q$, the Coulomb contributions are small and the results in both schemes agree.

With this modified counting, it is not straightforward to deduce the scaling of loops anymore. Kinetic energies always scale like Q , so the scaling of dq_0 and the nucleon propagator is not modified in the presence of Coulomb effects. However, where we could simply assume that all loop momenta scale like Q before, we now have to check first which contribution is picked up (or rather enhanced) after carrying out the dq_0 -integral. In general, we have that

1. the loop integration measure d^3q scales as q^3 , and
2. the photon propagator scales as $1/q^2$,

where either $q \sim Q$ or $q \sim p$. These rules will become more transparent when we apply them to deduce the scaling of the diagrams shown below.

3. Selected diagrams

In this subsection, we discuss several diagrams contributing to p - d scattering that include Coulomb photons (see Fig. 3). For the discussion we always assume $p \ll Q$. Diagram (a)

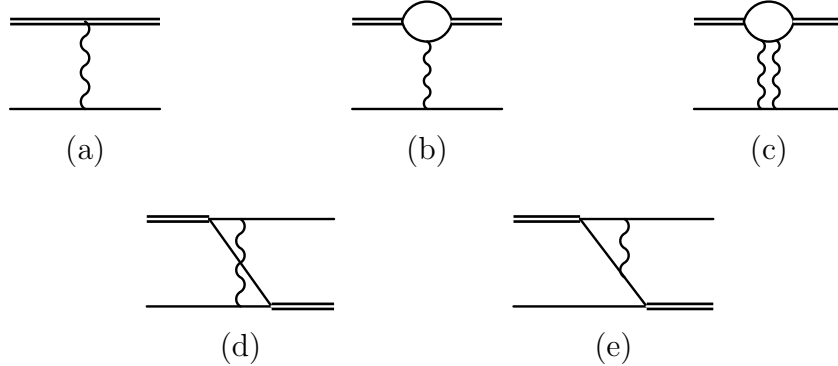


FIG. 3: Diagrams for p - d scattering involving the exchange of Coulomb photons.

simply scales as α/p^2 . The diagram (b) is enhanced relative to (a) by a factor Λ/Q from the nucleon bubble and hence gives the leading-order Coulomb contribution. Diagram (a) enters only at NLO since the dibaryon kinetic energy operators, which generate the direct coupling of the photons to the dibaryons, enter only as effective range corrections.

Diagram (c) contains two loops, which have to be analysed separately. The upper nucleon bubble does not contain any photon propagators, so there all momenta scale as Q . In the lower loop, momenta certainly scale $\sim p$ due to the two photon propagators that involve the external momentum. Including the remaining nucleon propagator, which cancels the contribution from the integration measure, we are left with a total scaling $\sim \alpha^2 M_N \Lambda / (Q^3 p)$ for diagram (c). This means that compared to diagram (b) it is suppressed by a factor $\alpha M_N p / Q^2$. For diagrams of the form (c) with more than two photons attached to the bubble we simply quote the results from [19]. The diagram with three photons could contribute with a factor $\sim \log(p/Q)$, whereas the diagrams with $n > 3$ photons attached to the bubble are even infrared finite and suppressed by factors α^n . Following [19], we neglect them all and also the logarithmically-scaling diagram with three photons (which is already small for $p \geq 1$ MeV).

Diagram (d) is a little ambiguous since *a priori* it is not clear whether the loop momentum should scale $\sim Q$ or $\sim p$. In [19], the first alternative is chosen, yielding that compared to the same diagram without the photon it is suppressed by a factor $\alpha M_N / Q$. A direct numerical calculation shows that it is a seven-percent effect at threshold.

The diagram (e) obviously is irrelevant for the quartet-channel system (there are never two protons in the dibaryon), but, at least in principle, it can play a role in the doublet-channel system. The power counting, however, yields the same suppression factor as for diagram (c), only in this case the scaling of the loop momentum is not ambiguous. A direct numerical evaluation yields that at threshold it is a 15% contribution (again compared to the simple nucleon-exchange diagram without the photon). We take this value as the *a priori* theoretical uncertainty of our doublet-channel calculation.

The bottom line of the discussion above is that, as done in [19], we iterate the diagrams (a) and (b) to all orders and do not include any of the other diagrams shown in Fig. 3. The claim is that this procedure is adequate for both the quartet-channel and the doublet-channel system. The Coulomb effects are thus included at NLO accuracy in our calculation.

III. SCATTERING EQUATIONS

A. Quartet channel

We start with a review of N - d quartet-channel scattering, where the spin 1 of the deuteron and the spin $1/2$ of the nucleon couple to a total spin of $3/2$. Since this coupling is only possible when the spins of all three nucleons taking part in the reaction are aligned, the Pauli principle applies. Hence, the system is rather insensitive to short-range physics. Furthermore, only the dibaryon field representing the deuteron can appear in the intermediate state.

Neutron–deuteron system

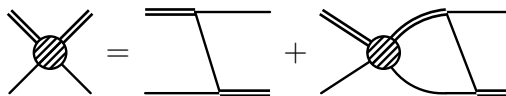


FIG. 4: Integral equation for the strong scattering amplitude \mathcal{T}_s in the quartet channel.

In Fig. 4 we show a diagrammatic representation of the strong (neutron–deuteron) scattering amplitude \mathcal{T}_s , which does not include any Coulomb effects. It is projected onto the spin quartet channel by setting $i = (1 - i2)/\sqrt{2}$ and $j = (1 + i2)/\sqrt{2}$ for the in- and outgoing deuteron spin indices, respectively, and $a = b = 2$ to select the neutron. After furthermore projecting onto S-waves, we get

$$\begin{aligned} \mathcal{T}_s^q(E; k, p) = & -\frac{M_N y_d^2}{kp} Q \left(\frac{k^2 + p^2 - M_N E - i\varepsilon}{kp} \right) \\ & + \frac{1}{2\pi^2} \int_0^\Lambda \frac{d^3 q}{(2\pi)^3} q^2 \mathcal{T}_s^q(E; k, q) \Delta_d \left(E - \frac{q^2}{2M_N}, q \right) \\ & \times \frac{M_N y_d^2}{qp} Q \left(\frac{q^2 + p^2 - M_N E - i\varepsilon}{qp} \right), \end{aligned} \quad (16)$$

where k and p are the incoming and outgoing momenta of the particles in the center-of-mass frame, and

$$Q(a) = \frac{1}{2} \int_{-1}^1 \frac{dx}{x+a} = \frac{1}{2} \log \left(\frac{a+1}{a-1} \right). \quad (17)$$

More details on the derivation of this equation and the required projections can be found in Appendix A. We have introduced a cutoff Λ to regularise the loop integral, which is particularly convenient for a numerical treatment of the equation. Strictly, however, this regulator is only required for the full amplitude including Coulomb interactions and is applied here for convenience only. After setting the energy E to the total center-of-mass energy,

$$E_k = \frac{3k^2}{4M_N} - \frac{\gamma_d^2}{M_N}, \quad (18)$$

the equation is solved numerically with standard linear algebra routines after discretising the integrals. From the result we then obtain the S-wave scattering phase shift

$$\delta(k) = \frac{1}{2i} \log \left(1 + \frac{2ikM_N}{3\pi} Z_0 \mathcal{T}(E_k; k, k) \right), \quad (19)$$

which can be compared to experimental data.

In order to simplify the expressions in the following sections, we introduce a short-hand notation for the scattering equations. Defining

$$D_{d,t}(E; q) \equiv \Delta_{d,t} \left(E - \frac{q^2}{2M_N}, q \right) \quad (20)$$

and

$$K_s(E; k, p) \equiv \frac{1}{kp} Q \left(\frac{k^2 + p^2 - M_N E - i\varepsilon}{kp} \right), \quad (21)$$

along with the operation

$$A \otimes B \equiv \frac{1}{2\pi^2} \int_0^\Lambda dq q^2 A(\dots, q) B(q, \dots), \quad (22)$$

we find that we can write (16) as

$$\mathcal{T}_s^q = -M_N y_d^2 K_s + \mathcal{T}_s^q \otimes [M_N y_d^2 D_d K_s], \quad (23)$$

where we have omitted all arguments.

Proton–deuteron system

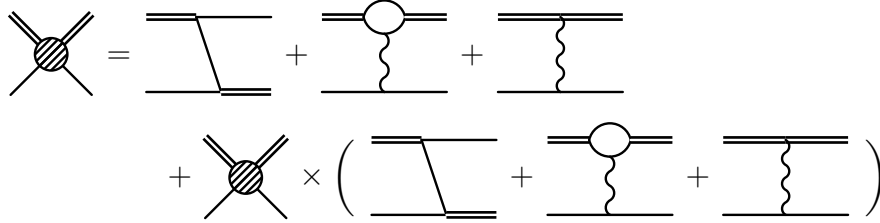


FIG. 5: Integral equation for the full (*i.e.* strong + Coulomb) scattering amplitude $\mathcal{T}_{\text{full}}$ in the quartet channel.

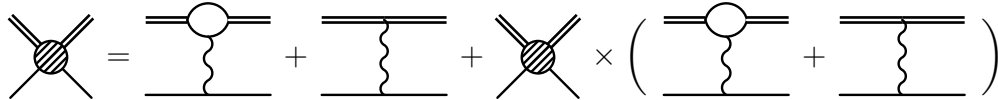


FIG. 6: Integral equation for the Coulomb scattering amplitude \mathcal{T}_c .

In order to include Coulomb effects and hence discuss proton–deuteron scattering we follow [19] and define a full scattering amplitude $\mathcal{T}_{\text{full}}$ (see Fig. 5) that includes both strong and Coulomb interactions and a pure Coulomb scattering amplitude \mathcal{T}_c (see Fig. 6). After spin-, isospin- and S-wave projection we find the integral equations

$$\mathcal{T}_{\text{full}}^q = -M_N y_d^2 \left(K_s - \frac{1}{2} K_c^{(d)} \right) + \mathcal{T}_{\text{full}}^q \otimes \left[M_N y_d^2 D_d \left(K_s - \frac{1}{2} K_c^{(d)} \right) \right] \quad (24)$$

and

$$\mathcal{T}_c^q = \frac{M_N y_d^2}{2} K_c^{(d)} - \mathcal{T}_c^q \otimes \left[\frac{M_N y_d^2}{2} D_d K_c^{(d)} \right] \quad (25)$$

with

$$K_c^{(d,t)}(E; k, p) = \frac{\alpha M_N}{2kp} Q \left(-\frac{k^2 + p^2 + \lambda^2}{2kp} \right) \left(\frac{1}{|\gamma_d|} - \rho_{d,t} \right). \quad (26)$$

After solving the individual equations, we calculate the phase shifts δ_{full} and δ_c according to (19). The final result, which we will compare to experimental data, is the Coulomb-subtracted phase shift [19, 27, 28],

$$\delta_{\text{diff}}(k) \equiv \delta_{\text{full}}(k) - \delta_c(k). \quad (27)$$

Note that in the integral equations above an artificial dependence on the bare coupling constant y_d is kept for notational convenience. In all observables, this dependence drops out.

B. Doublet channel

We now go on to the doublet channel, where the spins of the nucleon and the deuteron couple to a total spin of $1/2$. The spin-singlet dibaryon can now appear in the intermediate state, which leads to two coupled amplitudes that differ in the type of the outgoing dibaryon. In contrast to the quartet channel, the three nucleon spins no longer need to be aligned in the same direction, which means that a non-derivative three-nucleon interaction is no longer prohibited by the Pauli principle. This channel is expected to be more sensitive to short-range physics in general, and in fact the three-body interaction (6) is *needed* at leading order to ensure correct renormalisation [22].

Neutron–deuteron system

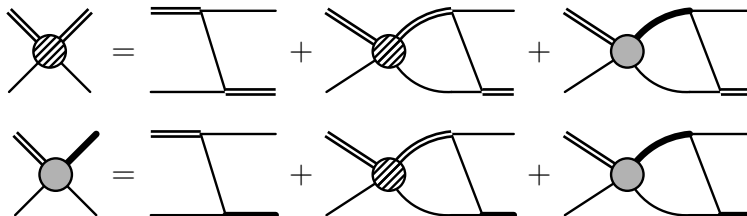


FIG. 7: Coupled-channel integral equation for the strong scattering amplitude \mathcal{T}_s in the doublet channel. The diagrams involving the three-body force have been omitted.

As we did in the quartet channel, we look at the neutron–deuteron system first. Fig. 7 shows a diagrammatic representation of the coupled-channel integral equation for the scattering amplitude \mathcal{T}_s , of which we only needed to consider the upper left part for the quartet-channel system. The contribution of the three-body interaction (6) is omitted here and will

be included below. After projecting onto the n - d doublet channel with

$$\mathcal{T}_s^{\text{d,a}} = \frac{1}{3} (\sigma^i)_{\alpha}^{\alpha'} (\mathcal{T}_s^{\text{a,ij}})^{\beta'b} (\sigma^j)_{\beta'}^{\beta} \Big|_{\substack{a=b=2 \\ \alpha=\beta=1}}, \quad (28\text{a})$$

$$\mathcal{T}_s^{\text{d,b}} = \frac{1}{3} (\sigma^i)_{\alpha}^{\alpha'} (\mathcal{T}_s^{\text{b,iB}})^{\beta'b'} (\tau^B)_{b'}^b \Big|_{\substack{a=b=2 \\ \alpha=\beta=1}}, \quad (28\text{b})$$

we find

$$\mathcal{T}_s^{\text{d,a}} = \frac{M_N y_d^2}{2} K_s - \mathcal{T}_s^{\text{d,a}} \otimes \left[\frac{M_N y_d^2}{2} D_d K_s \right] + \mathcal{T}_s^{\text{d,b}} \otimes \left[\frac{3 M_N y_d y_t}{2} D_t K_s \right], \quad (29\text{a})$$

$$\mathcal{T}_s^{\text{d,b}} = -\frac{3 M_N y_d y_t}{2} K_s + \mathcal{T}_s^{\text{d,a}} \otimes \left[\frac{3 M_N y_d y_t}{2} D_d K_s \right] - \mathcal{T}_s^{\text{d,b}} \otimes \left[\frac{M_N y_t^2}{2} D_t K_s \right]. \quad (29\text{b})$$

More details on the derivation and projection are again given in Appendix A.

Three-nucleon force

We still need to include the contribution of the three-nucleon interaction (6) in Eqs. (29a) and (29b). A straightforward calculation shows that this can be achieved with the replacement [22]

$$K_s(E; k, p) \rightarrow K_s(E; k, p) + \frac{2H(\Lambda)}{\Lambda^2}. \quad (30)$$

It is, however, important to note that for the terms with an additional factor of 3 in front of K_s , it is cancelled in the $H(\Lambda)$ -part by the additional factor 1/3 in (6). With this, we arrive at the final version of our integral equations,

$$\begin{pmatrix} \mathcal{T}_s^{\text{d,a}} \\ \mathcal{T}_s^{\text{d,b}} \end{pmatrix} = \begin{pmatrix} g_{dd} \left(K_s + \frac{2H(\Lambda)}{\Lambda^2} \right) \\ -g_{dt} \left(3K_s + \frac{2H(\Lambda)}{\Lambda^2} \right) \end{pmatrix} + \begin{pmatrix} -g_{dd} D_d \left(K_s + \frac{2H(\Lambda)}{\Lambda^2} \right) & g_{dt} D_t \left(3K_s + \frac{2H(\Lambda)}{\Lambda^2} \right) \\ g_{dt} D_d \left(3K_s + \frac{2H(\Lambda)}{\Lambda^2} \right) & g_{tt} D_t \left(K_s + \frac{2H(\Lambda)}{\Lambda^2} \right) \end{pmatrix} \otimes \begin{pmatrix} \mathcal{T}_s^{\text{d,a}} \\ \mathcal{T}_s^{\text{d,b}} \end{pmatrix}, \quad (31)$$

written in a compact matrix–vector notation. We have furthermore introduced the abbreviations

$$g_{dd} = \frac{M_N y_d^2}{2}, \quad g_{dt} = \frac{M_N y_d y_t}{2}, \quad g_{tt} = \frac{M_N y_t^2}{2}. \quad (32)$$

Again, the dependence on the bare coupling constants y_d and y_t is only kept for notational convenience and drops out in all observables.

Proton–deuteron system

Finally, we have all the ingredients to discuss the proton–deuteron system in the doublet channel.

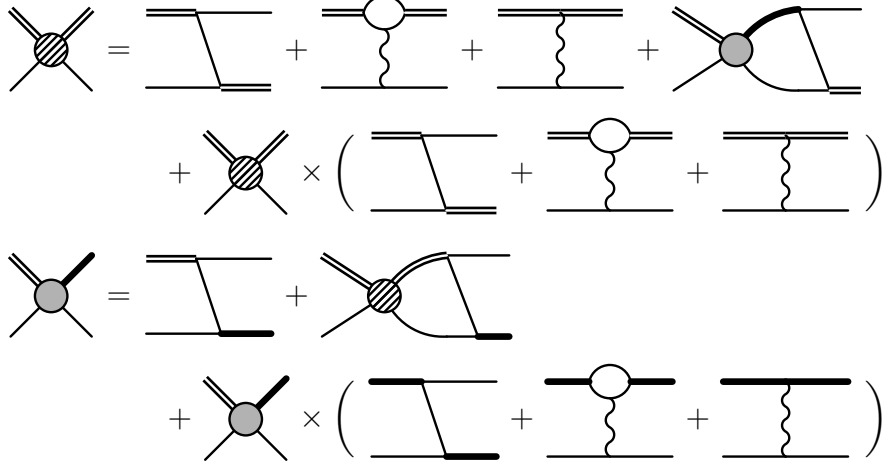


FIG. 8: Coupled-channel integral equation for the full (*i.e.* strong + Coulomb) scattering amplitude $\mathcal{T}_{\text{full}}$ in the doublet channel. The diagrams representing the three-nucleon force have been omitted.

Due to the fact that the electromagnetic interaction does not couple to isospin eigenstates we now need two different projections for the amplitude \mathcal{T}^b with the outgoing spin-singlet dibaryon:

$$\mathcal{T}_{\text{full}}^{\text{d},\text{b1}} = \frac{1}{3} (\sigma^i)_{\alpha}^{\alpha'} (\mathcal{T}_{\text{full}}^{\text{b},iB})_{\alpha'a}^{\beta b'} (\mathbf{1} \cdot \delta^{B3})_{b'}^b \Big|_{\substack{a=b=1 \\ \alpha=\beta=1}}, \quad (33\text{a})$$

$$\mathcal{T}_{\text{full}}^{\text{d},\text{b2}} = \frac{1}{3} (\sigma^i)_{\alpha}^{\alpha'} (\mathcal{T}_{\text{full}}^{\text{b},iB})_{\alpha'a}^{\beta b'} (\mathbf{1} \cdot \delta^{B1} + i\mathbf{1} \cdot \delta^{B2})_{b'}^b \Big|_{\substack{a=1, b=2 \\ \alpha=\beta=1}}. \quad (33\text{b})$$

The latter corresponds to the amplitude with the outgoing spin-singlet dibaryon in a pure pp -state. For the diagrams that have this component in the intermediate state, we have to insert the propagator (12) into the unprojected equations in Appendix A and find

$$\begin{aligned} \begin{pmatrix} \mathcal{T}_{\text{full}}^{\text{d},\text{a}} \\ \mathcal{T}_{\text{full}}^{\text{d},\text{b1}} \\ \mathcal{T}_{\text{full}}^{\text{d},\text{b2}} \end{pmatrix} &= \begin{pmatrix} g_{dd} \left(K_s + \frac{2H(\Lambda)}{\Lambda^2} \right) \\ -g_{dt} \left(K_s + \frac{2H(\Lambda)}{3\Lambda^2} \right) \\ -g_{dt} \left(2K_s + \frac{4H(\Lambda)}{3\Lambda^2} \right) \end{pmatrix} + \begin{pmatrix} g_{dd} K_c^{(d)} \\ 0 \\ 0 \end{pmatrix} \\ &+ \begin{pmatrix} -g_{dd} D_d \left(K_s + \frac{2H(\Lambda)}{\Lambda^2} \right) & g_{dt} D_t \left(3K_s + \frac{2H(\Lambda)}{\Lambda^2} \right) & 0 \\ g_{dt} D_d \left(K_s + \frac{2H(\Lambda)}{3\Lambda^2} \right) & g_{tt} D_t \left(K_s + \frac{2H(\Lambda)}{\Lambda^2} \right) & 0 \\ g_{dt} D_d \left(2K_s + \frac{4H(\Lambda)}{3\Lambda^2} \right) & -g_{tt} D_t \left(2K_s + \frac{4H(\Lambda)}{\Lambda^2} \right) & 0 \end{pmatrix} \otimes \begin{pmatrix} \mathcal{T}_{\text{full}}^{\text{d},\text{a}} \\ \mathcal{T}_{\text{full}}^{\text{d},\text{b1}} \\ \mathcal{T}_{\text{full}}^{\text{d},\text{b2}} \end{pmatrix} \\ &+ \begin{pmatrix} -g_{dd} D_d K_c^{(d)} & 0 & g_{dt} D_t^{pp} \left(3K_s + \frac{2H(\Lambda)}{\Lambda^2} \right) \\ 0 & -g_{tt} D_t K_c^{(t)} & -g_{tt} D_t^{pp} \left(K_s + \frac{2H(\Lambda)}{\Lambda^2} \right) \\ 0 & 0 & 0 \end{pmatrix} \otimes \begin{pmatrix} \mathcal{T}_{\text{full}}^{\text{d},\text{a}} \\ \mathcal{T}_{\text{full}}^{\text{d},\text{b1}} \\ \mathcal{T}_{\text{full}}^{\text{d},\text{b2}} \end{pmatrix} \quad (34) \end{aligned}$$

with

$$D_t^{pp}(E; q) \equiv \Delta_{t,pp} \left(E - \frac{q^2}{2M_N}, q \right). \quad (35)$$

The terms in (34) have been separated in such a way that the sub-channels with Coulomb contributions can be easily identified. The equation for the Coulomb scattering amplitude \mathcal{T}_c is exactly the same as in the quartet channel.

C. Higher order corrections

The dibaryon propagators with the resummed kinetic energy insertions have an unphysical deep bound state pole at the radius of convergence of the geometric series. In the quartet channel the cutoff can be chosen low enough to avoid that pole. Due to the larger cutoff needed in the doublet channel, however, we cannot use the resummed propagators here. Instead, we use linear and quadratic insertions of the kinetic energy operator in the kernel of the integral equations in order to include effective range corrections and obtain the next-to-leading order and next-to-next-to-leading order propagators $D_{d,t}^{\text{NLO}}$ and $D_{d,t}^{\text{N}^2\text{LO}}$ [23]. Alternatively, we can think of this as re-expanding the renormalised propagators (9) and (10) up to linear and quadratic order in $\rho_{d,t}$, respectively. This still resums some higher order effective range contributions, but removes the unphysical pole.

The question of when higher-order three-body forces enter in the doublet channel is still under discussion. In Ref. [23], a subleading three-body force was included as required by naïve dimensional analysis. A Lepage-plot analysis showed that its inclusion reduces the errors in the calculation. This was supported by Ref. [29], where a corresponding logarithmic divergence at N²LO, requiring a subleading three-body force, was identified. More recently, Platter and Phillips, using the subtractive renormalisation scheme, showed that the leading three-body force is sufficient to achieve cutoff independence up to N²LO [30]. A perturbative analysis recently showed that there is a new three-body parameter already at NLO if the scattering length is not fixed [31]. In this work, the scattering length *is* fixed and we will not include a subleading three-body force. Assuming the counting of [23], our calculation will correspond to N²LO in the quartet channel and to NLO in the doublet channel. We will also perform a calculation including only the two-body interactions to N²LO in the doublet channel.

D. Numerical implementation

The integral equations presented in the previous sections have to be solved numerically. We do so by discretising the integrals, using Gaussian quadrature, principal value integration to deal with the singularity of the deuteron propagator, and appropriate transformations of the integration domain.

The latter are especially important to deal with the numerical difficulties caused by the Coulomb photon propagators. Even though we have regulated the singularity with the artificial photon mass λ , the latter has to be kept small, which then yields strongly peaked functions. It turns out that the Coulomb peaks in the inhomogeneous parts of Eqs. (24), (25) and (34) are the major numerical problem. We solve it by concentrating the quadrature points around this peak. Together with always putting half of the quadrature points into the low-momentum region (the interval from zero to the peak position), we are able to (linearly) extrapolate our results for the scattering phase shifts back to the physical value $\lambda = 0$ (screening limit). As a typical example, we show the quartet-channel phase shift at $k = 5$ MeV as a function of λ in Fig. 9. The linear dependence is clearly visible, with

deviations only for very small λ . In the doublet channel, the qualitative behaviour is the same, only the curvature becomes visible already for somewhat larger photon masses. This can be understood by noting that the absolute value of the phase shift is smaller in the doublet channel, especially for low center-of-mass momenta k (*cf.* Sec. IV). We settled to use the intervals $0.1 \leq \lambda \leq 0.15$ and $0.4 \leq \lambda \leq 0.6$ for the extrapolations in the quartet and doublet channel, respectively. We note that the error introduced by the extrapolation to $\lambda = 0$ can generally be neglected compared to the theoretical error from the EFT expansion discussed below.

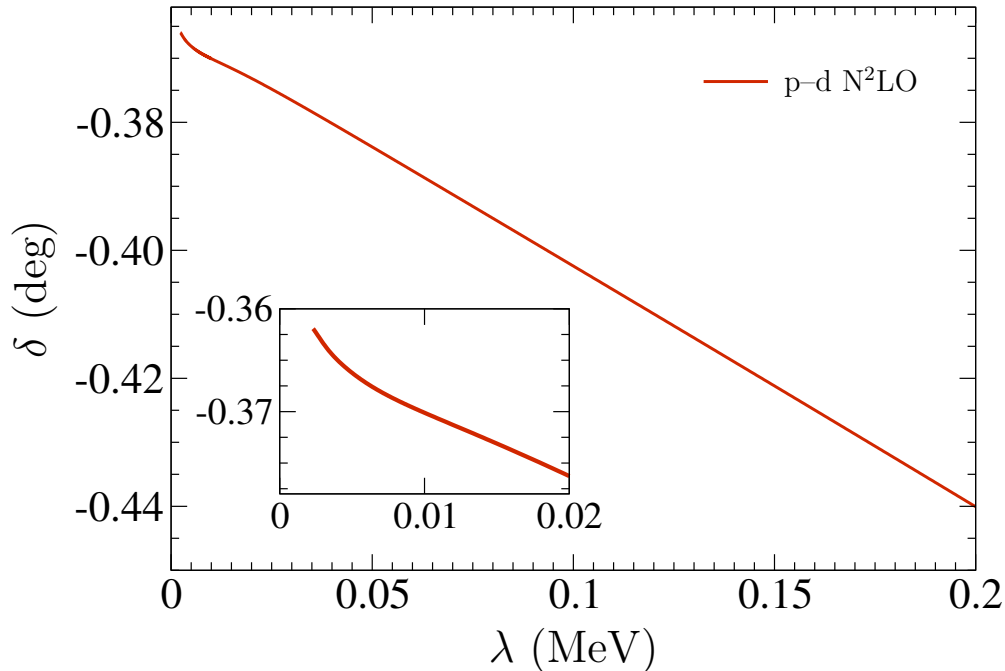


FIG. 9: p - d quartet channel S-wave scattering phase shift at N²LO for center-of-mass momentum $k = 5$ MeV and cutoff $\Lambda = 140$ MeV as a function of the regulating photon mass λ .

We have used the experimental input parameters shown in Tab. I in the numerical calculation.

Parameter	Value	Parameter	Value
γ_d	45.701 MeV [32]	ρ_d	1.765 fm [33]
a_t	-23.714 fm [2]	ρ_t	2.73 fm [2]
a_C	-7.8063 fm [34]	r_C	2.794 fm [34]

TABLE I: Parameters used in the numerical calculation, $\gamma_d = \sqrt{M_N E_B^d}$.

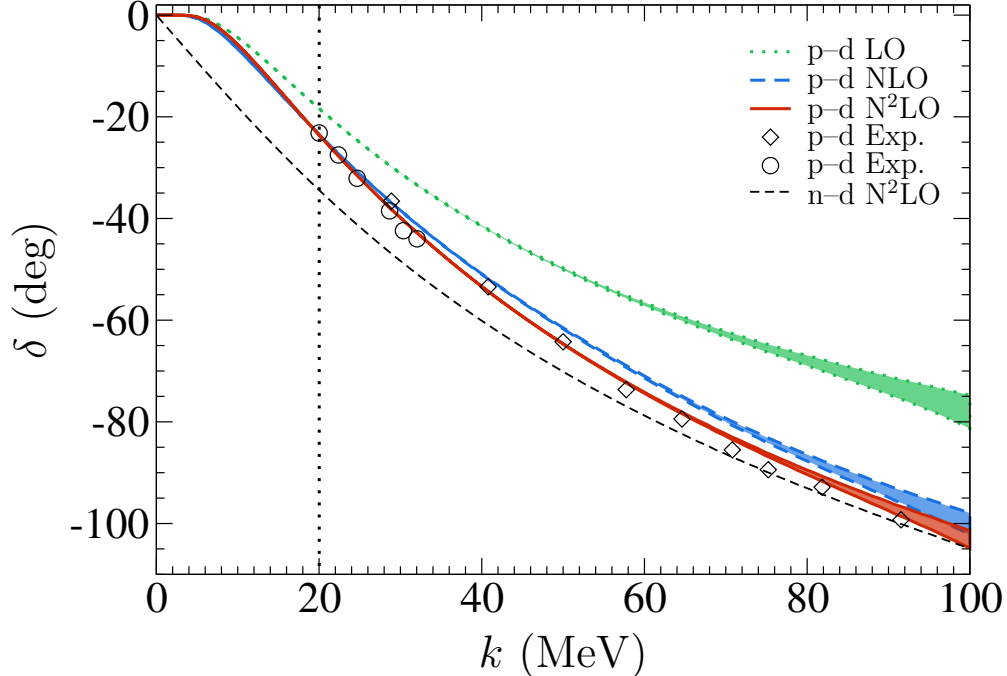


FIG. 10: N - d quartet channel S-wave scattering phase shifts as functions of the center-of-mass momentum k . Error bands generated by cutoff variation from 120 to 160 MeV. Experimental p - d phase shift data taken from [35] (diamonds) and [36] (circles).

IV. SCATTERING RESULTS

A. Quartet channel

In Fig. 10 we show the phase shift results for both neutron–deuteron and proton–deuteron scattering as functions of the center-of-mass momentum k . The error bands are generated by varying the cutoff within a range of 120 to 160 MeV. Since the cutoff variation is small, we conclude that the calculation is well converged at these cutoffs. For $\Lambda \gtrsim 200$ MeV some numerical artifacts show up from integrating over the unphysical second pole in the full deuteron propagator. For the n - d curve in Fig. 10 we have used $\Lambda = 140$ MeV. The fact that the bands do not overlap is no point of concern since they only give a lower bound on the error of the calculation. From the expansion parameter $\gamma_d \rho_d \approx 1/3$ of the EFT, the error can be estimated as 30%, 10%, and 3% at LO, NLO, and N²LO, respectively. Thus, at LO, the 30% error from the expansion parameter clearly dominates. At NLO and N²LO, however, the band from the cutoff variation gives a reasonable estimate of the total error in the calculation.

The N²LO result to the right of the dotted line at $k = 20$ MeV agrees nicely with the results presented in [19] and also with the experimental data included in the plot. At this point we remark, however, that for $k \gtrsim 20$ MeV the Coulomb parameter $\alpha M_N/k$ is of order 1/3, which means that in this regime the non-perturbative treatment of Coulomb effects might not even be necessary. More important are hence the p - d results for small momenta ($k < 20$ MeV) to the left of the dotted line, which we could obtain thanks to our optimised numerical procedure. It would of course be good to have some data points in this region to

test our prediction.

B. Doublet channel

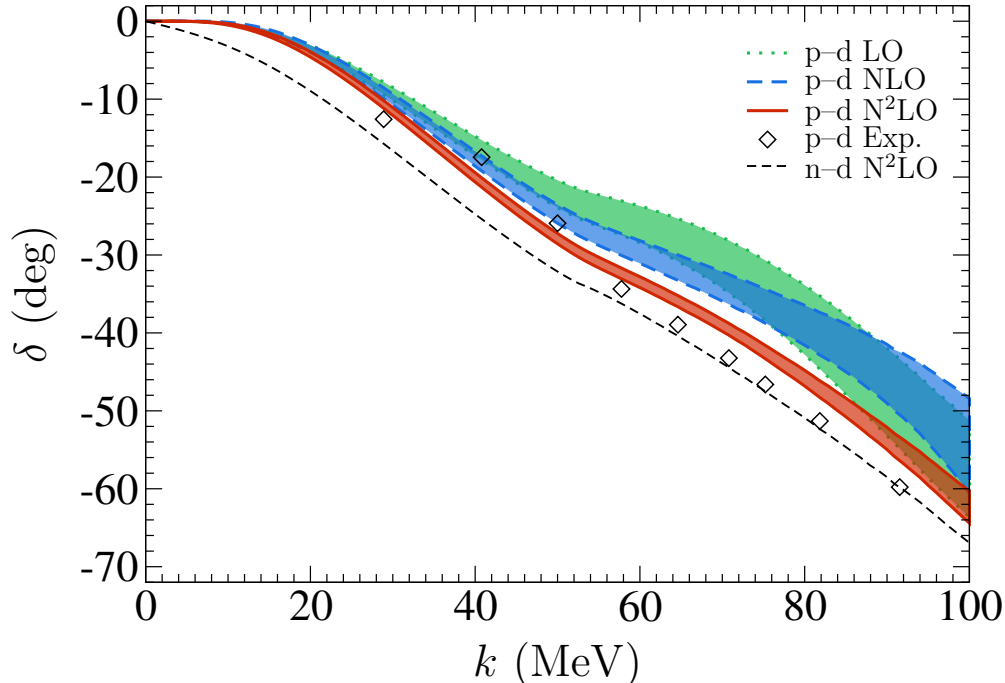


FIG. 11: N - d doublet channel S-wave scattering phase shifts as functions of the center-of-mass momentum k . Error bands generated by cutoff variation from 200 to 600 MeV. Experimental p - d phase shift data taken from [35].

The doublet-channel results for the p - d scattering phase shifts as functions of the center-of-mass momentum k are shown in Fig. 11. As in the quartet channel, the p - d curve lies above the n - d curve and agrees quite well with the experimental data. A more quantitative comparison is, unfortunately, not possible since there are no errors given for the data points. The error bands are generated by varying the cutoff within a natural range of 200 to 600 MeV (*i.e.* a few times the pion mass). Assuming the power counting of [23], our N²LO calculation is incomplete since the subleading three-body force is not included. A full calculation, however, is beyond the scope of the paper since gauging the subleading three-body force creates new three-body contributions to the photon coupling. Our partial N²LO result is stable to within about ten percent under the cutoff variation, which is consistent with a 7–15% error estimate based on the neglected Coulomb diagrams (see Sec. IID and [19]).

Figure 11 furthermore shows how the results improve from order to order. The stability of the partial N²LO result with respect to variation of the cutoff suggests that the scattering is relatively insensitive to the subleading three-body interaction. At higher energies, however, there is some room for such a contribution as our partial result consistently lies two to four degrees above the data.

We observe that the shift from LO to NLO is of the same order of magnitude as the shift from NLO to N²LO. This behaviour is typical for effective range corrections in the

doublet channel [37]. The smallness of the NLO corrections can be understood as a cancellation between two different contributions to this correction. The two contributions are proportional to $\kappa\rho_d$ and $\gamma_d\rho_d$, respectively, where κ is the typical momentum scale of the process. Furthermore, it is known that at LO observables are often described better than expected from the power counting once the exact pole position of the two-body propagator is reproduced [24]. As a consequence, the shifts in observables from LO to NLO can be small and of a size comparable to the corresponding shifts from NLO to N²LO.

V. ³HE BOUND STATE PROPERTIES

Since the power counting we used for the Coulomb contributions is not valid for the regime of typical bound state energies, we cannot simply use the above equations to calculate ³He. There are various strategies to proceed. We could extend the power counting and include additional Coulomb diagrams in our equations. Alternatively, we could use an analytic expression for the full off-shell Coulomb amplitude as it is done in Ref. [20] for an LO calculation. Here, we choose the much simpler approach of calculating the Coulomb energy shift for ³He in first order perturbation theory as the expectation value of the Coulomb interaction between proton and deuteron using trinucleon wave functions in the isospin limit.

A. Trinucleon wave functions

In order to obtain the trinucleon wave functions we need to solve the homogeneous coupled-channel equation

$$\vec{\mathcal{B}}_s = (\hat{K}\hat{D}) \otimes \vec{\mathcal{B}}_s \quad (36)$$

with $\vec{\mathcal{B}}_s \equiv (\mathcal{B}_s^{\text{d,a}}, \mathcal{B}_s^{\text{d,b1}}, \mathcal{B}_s^{\text{d,b2}})^T$, $\hat{D} = \text{diag}(D_d, D_t, D_t)$, and

$$\hat{K} \equiv \begin{pmatrix} -g_{dd} \left(K_s + \frac{2H(\Lambda)}{\Lambda^2} \right) & g_{dt} \left(3K_s + \frac{2H(\Lambda)}{\Lambda^2} \right) & g_{dt} \left(3K_s + \frac{2H(\Lambda)}{\Lambda^2} \right) \\ g_{dt} \left(K_s + \frac{2H(\Lambda)}{3\Lambda^2} \right) & g_{tt} \left(K_s + \frac{2H(\Lambda)}{\Lambda^2} \right) & -g_{tt} \left(K_s + \frac{2H(\Lambda)}{\Lambda^2} \right) \\ g_{dt} \left(2K_s + \frac{4H(\Lambda)}{3\Lambda^2} \right) & -g_{tt} \left(2K_s + \frac{4H(\Lambda)}{\Lambda^2} \right) & 0 \end{pmatrix}. \quad (37)$$

It is obtained by applying the projections (33) to the raw equation without Coulomb contributions (A6). The reason to separate the wave function in this way is that the part with the dibaryon leg in the pp -channel does not contribute to a perturbative calculation of the energy shift since in that case the third nucleon in the system necessarily is a neutron. The energy in the equation is set to the experimental triton binding energy,

$$-E_B^{3\text{H}} = -8.48 \text{ MeV}, \quad (38)$$

and the existence of solution is ensured by adjusting the three-nucleon force $H(\Lambda)$ appropriately, as it was already done to renormalise the scattering equations.

Having obtained the wave functions as solutions of (36), we still need to normalise them properly. Since the EFT generates an energy-dependent interaction in the three-body system, this is done by demanding that

$$\left(\hat{D}\vec{\mathcal{B}}_s \right)^T \otimes \frac{d}{dE} \left(\hat{I} - \hat{K} \right) \Big|_{E=-E_B^{3\text{H}}} \otimes \left(\hat{D}\vec{\mathcal{B}}_s \right) = 1, \quad (39)$$

where $\hat{I} = \text{diag}(I_d, I_t, I_t)$ with

$$I_{d,t}(E, q, q') = \frac{2\pi^2}{q^2} \delta(q - q') D_{d,t}(E; q)^{-1}. \quad (40)$$

A short derivation of this normalisation condition can be found in Appendix B.

B. Perturbative ${}^3\text{He}$ energy shift

With the normalised trinucleon wave functions we can obtain the Coulomb-induced energy shift in first order perturbation theory and find

$$\Delta E = \left(\hat{D}\vec{\mathcal{B}}_s \right)^T \otimes \text{diag}(V_C, V_C, 0) \otimes \left(\hat{D}\vec{\mathcal{B}}_s \right) \quad (41)$$

with the S-wave projected Coulomb potential

$$V_C(E; q, q') = -\frac{4\pi\alpha}{2qq'} Q \left(-\frac{q^2 + q'^2 + \lambda^2}{2qq'} \right) \quad (42)$$

in momentum space. Our prediction for the ${}^3\text{He}$ binding energy is then given by

$$-E_B^{{}^3\text{He}} = -E_B^{{}^3\text{H}} + \Delta E. \quad (43)$$

C. Results

The results are shown in Fig. 12. It is remarkable that the NLO result, which should be accurate to about 10%, agrees very well with the experimental value

$$\Delta E_{\text{exp}} = 0.7629 \text{ MeV} \quad (44)$$

over a large cutoff range. In our partial N²LO calculation, the results are still quite stable against cutoff variations within 200 to about 400 MeV, but our value lies about 0.1 MeV above the experimental value. This shift again leaves room for a natural-sized contribution of the subleading three-body we have not included.

Brandenburger, Coon and Sauer have determined the ${}^3\text{He}$ – ${}^3\text{H}$ binding energy difference in a largely model-independent way using experimental charge form factors [38]. They found that the Coulomb contribution is about 10% below the experimental value for the total energy difference. Within the expected error of 10%, our NLO result is consistent with this. Ando and Birse have carried out a non-perturbative calculation to leading order in the pionless EFT including the full off-shell \mathcal{T} -matrix for the Coulomb interaction and found $\Delta E = 0.82$ MeV [20]. Their calculation included isospin breaking effects in the nucleon–nucleon scattering lengths. Kirscher *et al.* found the smaller value $\Delta E = 0.66 \pm 0.03$ MeV in an NLO calculation using the resonating group model to solve the pionless EFT with a charge-independent value of the spin-singlet scattering length and non-perturbative Coulomb interactions [21].

The increase in our N²LO result for $\Lambda \gtrsim 400$ MeV that is seen in Fig. 12 also occurs at LO and NLO, but for larger cutoffs. In Fig. 13 we show the NLO prediction for $E_B^{{}^3\text{He}}$ together

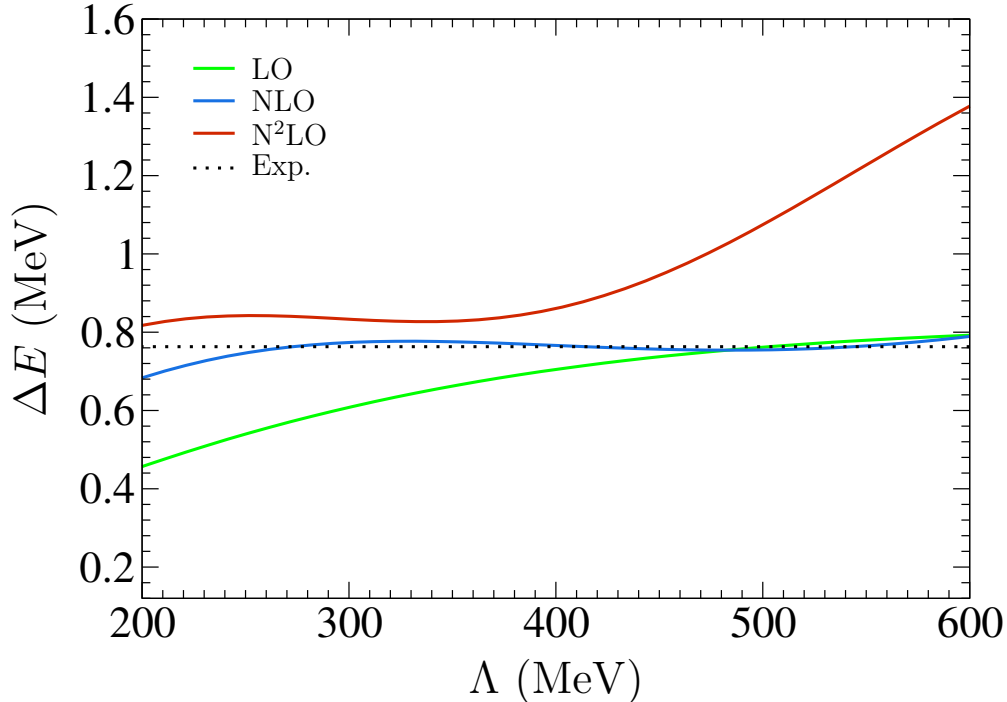


FIG. 12: Perturbative prediction for the ${}^3\text{He}$ – ${}^3\text{H}$ binding energy difference in dependence of the cutoff Λ . Bottom curve: LO result. Middle curve: NLO result. Top curve: N^2LO result.

with the three-nucleon force obtained from fitting the triton binding energy. It is obvious that a drop in the binding energy prediction occurs whenever the three-nucleon force has gone through a pole. We interpret this as an artifact of the theory which is related to the Efimov effect. For cutoffs beyond the position of the first pole in $H(\Lambda)$, the triton is not the true ground state of the system anymore; after each pole transition a new (unphysical) deep bound state emerges.

These unphysical deep states lead to additional nodes in the triton wave function at short distances which affect our perturbative results. This suggests that an additional short-distance counterterm is required to cancel these contributions if one wants to go to cutoffs much larger than the pion mass.

VI. SUMMARY AND OUTLOOK

In this paper, we have investigated S-wave proton–deuteron scattering in pionless effective field theory. In the quartet channel, we have calculated the elastic scattering phase shift up to N^2LO using the power counting for Coulomb contributions suggested by Rupak and Kong [19]. The Coulomb effects are included at NLO accuracy in our calculation. Using an optimised integration mesh we were able to extend their calculation into the threshold region where the Coulomb interaction becomes highly non-perturbative. We found good agreement both with available phase shift analyses and with the results of Rupak and Kong at momenta $k \geq 20$ MeV.

Moreover, we extended the power counting to the doublet channel and performed a complete calculation of the phase shifts to NLO in agreement with the available phase shift

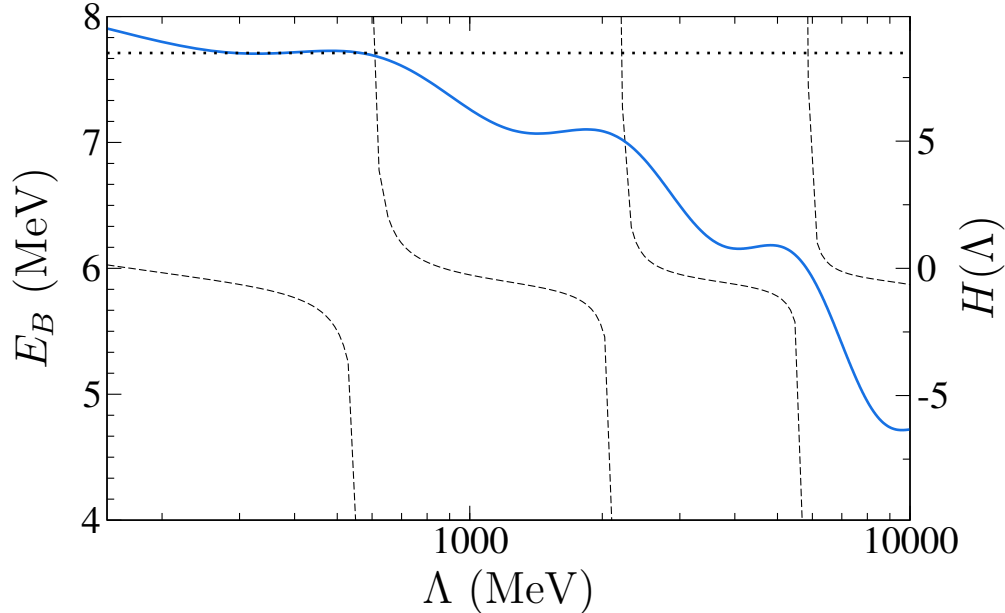


FIG. 13: Perturbative prediction for the ${}^3\text{He}$ binding energy together with the three-nucleon force; NLO results. Solid curve: ${}^3\text{He}$ binding energy prediction. Dashed curve: three-nucleon force. Dotted line: experimental value for the ${}^3\text{He}$ binding energy.

data. We also carried out a partial N²LO calculation that neglected the contribution of the subleading three-body force entering at this order. The results of this calculation are stable under variations of the cutoff. Furthermore, there is good agreement with the phase shift data at low momenta and room for a small contribution of the neglected three-body force at larger momenta. Overall, however, the doublet channel phase shifts are only weakly sensitive to the subleading three-body force entering at N²LO.

Although we were mainly interested in p - d scattering, we have also calculated the Coulomb contribution to the ${}^3\text{He}$ - ${}^3\text{H}$ binding energy difference ΔE . This observable has previously been calculated in the pionless theory by treating the Coulomb interaction non-perturbatively [20, 21]. Here, we treat the Coulomb potential between proton and deuteron in first order perturbation theory using trinucleon wave functions. Higher order corrections to this quantity are expected to be small. Our NLO result is in reasonable agreement with the experimental value and other evaluations. We find ΔE to be more sensitive to the subleading three-body force. The partial N²LO result is about 10% too large, thus leaving room for a contribution from the omitted three-body force. We also observe steps in the calculated value of ΔE as the cutoff is increased beyond its natural range. Whenever the leading three-nucleon force has gone through a pole, a drop in the calculated binding energy occurs. We interpret this as an artifact of the theory related to the Efimov effect. At higher cutoffs, spurious deep three-body bound states appear and the triton is not the true ground state anymore. It appears that an additional short-distance counterterm is required to cancel these contributions if one wants to go to cutoffs much larger than the pion mass. A further study of this issue would be interesting.

In the future, a full N²LO calculation including the subleading three-body force and the electromagnetic interaction terms generated from gauging its momentum dependence should be carried out. Such an accuracy will, *e.g.*, be required for high-precision calculations of

low-energy astrophysical processes in pionless effective field theory and the effective field theory for halo nuclei.

Acknowledgments

We thank A. Rusetsky, B. Metsch, M. Hoferichter and P. Hagen for discussions and S.-I. Ando, S. Coon, D. R. Phillips and U. van Kolck for comments on the manuscript. This research was supported in part by the DFG through SFB/TR 16 ‘‘Subnuclear structure of matter’’ and the BMBF under contract No. 06BN9006. S.K. was supported by the ‘‘Studienstiftung des deutschen Volkes’’ and by the Bonn-Cologne Graduate School of Physics and Astronomy.

Appendix A: Scattering equation details

1. Quartet channel

Using the Feynman rules that follow from the Lagrangian (1) and inserting appropriate symmetry factors, we find

$$\begin{aligned}
(i\mathcal{T}_s^{ij})_{\alpha a}^{\beta b}(E; \mathbf{k}, \mathbf{p}) &= -\frac{iM_N y_d^2}{2} \cdot (\sigma^j \sigma^i)_\alpha^\beta \delta_a^b \cdot \frac{1}{\mathbf{k}^2 + \mathbf{k} \cdot \mathbf{p} + \mathbf{p}^2 - M_N E - i\epsilon} \\
&+ \int \frac{d^3 q}{(2\pi)^3} \Delta_d \left(E - \frac{\mathbf{q}^2}{2M_N}, \mathbf{q} \right) \cdot (i\mathcal{T}_s^{ik})_{\alpha a}^{\gamma c}(E; \mathbf{k}, \mathbf{q}) \\
&\quad \times \frac{M_N y_d^2}{2} \frac{(\sigma^j \sigma^k)_\gamma^\beta \delta_c^b}{\mathbf{q}^2 + \mathbf{q} \cdot \mathbf{p} + \mathbf{p}^2 - M_N E - i\epsilon} \quad (\text{A1})
\end{aligned}$$

for the n - d scattering equation depicted in Fig. 4. In the same way we get

$$\begin{aligned}
(i\mathcal{T}_{\text{full}}^{ij})_{\alpha a}^{\beta b}(E; \mathbf{k}, \mathbf{p}) &= -\frac{iM_N y_d^2}{2} \cdot (\sigma^j \sigma^i)_\alpha^\beta \delta_a^b \cdot \frac{1}{\mathbf{k}^2 + \mathbf{k} \cdot \mathbf{p} + \mathbf{p}^2 - M_N E - i\epsilon} \\
&- i\alpha M_N^2 y_d^2 \cdot \delta^{ij} \delta_\alpha^\beta \left(\frac{\mathbf{1} + \tau_3}{2} \right)_a^b \left[\frac{\mathcal{I}_{\text{bubble}}(E; \mathbf{k}, \mathbf{p})}{(\mathbf{k} - \mathbf{p})^2 + \lambda^2} - \frac{\rho_d}{2} \frac{1}{(\mathbf{k} - \mathbf{p})^2 + \lambda^2} \right] \\
&+ \int \frac{d^3 q}{(2\pi)^3} \Delta_d \left(E - \frac{\mathbf{q}^2}{2M_N}, \mathbf{q} \right) \cdot (i\mathcal{T}_{\text{full}}^{ik})_{\alpha a}^{\gamma c}(E; \mathbf{k}, \mathbf{q}) \cdot \left\{ \frac{M_N y_d^2}{2} \frac{(\sigma^j \sigma^k)_\gamma^\beta \delta_c^b}{\mathbf{q}^2 + \mathbf{q} \cdot \mathbf{p} + \mathbf{p}^2 - M_N E - i\epsilon} \right. \\
&\quad \left. + \alpha M_N^2 y_d^2 \cdot \delta^{kj} \delta_\gamma^\beta \left(\frac{\mathbf{1} + \tau_3}{2} \right)_c^b \left[\frac{\mathcal{I}_{\text{bubble}}(E; \mathbf{q}, \mathbf{p})}{(\mathbf{q} - \mathbf{p})^2 + \lambda^2} - \frac{\rho_d}{2} \frac{1}{(\mathbf{q} - \mathbf{p})^2 + \lambda^2} \right] \right\} \quad (\text{A2})
\end{aligned}$$

for the full p - d scattering equation shown in Fig. 5, and

$$\begin{aligned}
(i\mathcal{T}_c^{ij})_{\alpha a}^{\beta b}(E; \mathbf{k}, \mathbf{p}) &= -i\alpha M_N^2 y_d^2 \cdot \delta^{ij} \delta_\alpha^\beta \left(\frac{\mathbf{1} + \tau_3}{2} \right)_a^b \left[\frac{\mathcal{I}_{\text{bubble}}(E; \mathbf{k}, \mathbf{p})}{(\mathbf{k} - \mathbf{p})^2 + \lambda^2} - \frac{\rho_d}{2} \frac{1}{(\mathbf{k} - \mathbf{p})^2 + \lambda^2} \right] \\
&+ \int \frac{d^3 q}{(2\pi)^3} \Delta_d \left(E - \frac{\mathbf{q}^2}{2M_N}, \mathbf{q} \right) \cdot (i\mathcal{T}_c^{ik})_{\alpha a}^{\gamma c}(E; \mathbf{k}, \mathbf{q}) \\
&\times \alpha M_N^2 y_d^2 \cdot \delta^{jk} \delta_\gamma^\beta \left(\frac{\mathbf{1} + \tau_3}{2} \right)_c^b \left[\frac{\mathcal{I}_{\text{bubble}}(E; \mathbf{q}, \mathbf{p})}{(\mathbf{q} - \mathbf{p})^2 + \lambda^2} - \frac{\rho_d}{2} \frac{1}{(\mathbf{q} - \mathbf{p})^2 + \lambda^2} \right] \quad (\text{A3})
\end{aligned}$$

for the pure Coulomb scattering equation (Fig. 6), where

$$\mathcal{I}_{\text{bubble}}(E; \mathbf{k}, \mathbf{p}) = \frac{\arctan \left(\frac{2\mathbf{p}^2 - \mathbf{k}^2 - \mathbf{k} \cdot \mathbf{p}}{\sqrt{3\mathbf{k}^2 - 4M_N E - i\varepsilon} \sqrt{(\mathbf{k} - \mathbf{p})^2}} \right) + \arctan \left(\frac{2\mathbf{k}^2 - \mathbf{p}^2 - \mathbf{k} \cdot \mathbf{p}}{\sqrt{3\mathbf{p}^2 - 4M_N E - i\varepsilon} \sqrt{(\mathbf{k} - \mathbf{p})^2}} \right)}{\sqrt{(\mathbf{k} - \mathbf{p})^2}} \quad (\text{A4})$$

corresponds to the loop integral in the diagram with the photon attached to a nucleon bubble. The expression looks quite complicated, but it can be simplified. The dominant terms of $\mathcal{I}_{\text{bubble}}$ are those with $\mathbf{p}^2 \approx \mathbf{k}^2$ and $\mathbf{p}^2 \approx \mathbf{q}^2$, respectively, due to the prefactors of $1/(\mathbf{k} - \mathbf{p})^2$ and $1/(\mathbf{q} - \mathbf{p})^2$. In the latter case we can furthermore assume that $\mathbf{q}^2 \approx \mathbf{k}^2$ because of the pole at this position in the propagator. Furthermore inserting the total center-of-mass energy $E = 3k^2/(4M_N) - \gamma_d^2/M_N$, we get

$$\frac{\mathcal{I}_{\text{bubble}}(E; \mathbf{k}, \mathbf{p})}{(\mathbf{k} - \mathbf{p})^2 + \lambda^2} \approx \frac{1}{2|\gamma_d|} \frac{1}{(\mathbf{k} - \mathbf{p})^2 + \lambda^2} \quad (\text{A5a})$$

and

$$\Delta_d \left(E - \frac{\mathbf{q}^2}{2M_N}, \mathbf{q} \right) \cdot \frac{\mathcal{I}_{\text{bubble}}(E; \mathbf{q}, \mathbf{p})}{(\mathbf{q} - \mathbf{p})^2 + \lambda^2} \approx \Delta_d \left(E - \frac{\mathbf{q}^2}{2M_N}, \mathbf{q} \right) \cdot \frac{1}{2|\gamma_d|} \frac{1}{(\mathbf{q} - \mathbf{p})^2 + \lambda^2}, \quad (\text{A5b})$$

where we have used (A4) and the expansion $\arctan(x) = x + \mathcal{O}(x^3)$. The same simplifications, which effectively amount to keeping only loop contributions with $q \sim p$, are used in [19] and appear to be well supported by comparing the results with experimental data (see Sec. IV).

2. Doublet channel

In the doublet channel we find

$$\begin{aligned}
(i\mathcal{T}_s^{a,ij})_{\alpha a}^{\beta b}(E; \mathbf{k}, \mathbf{p}) &= -\frac{iM_N y_d^2}{2} \cdot (\sigma^j \sigma^i)_\alpha^\beta \delta_a^b \cdot \frac{1}{\mathbf{k}^2 + \mathbf{k} \cdot \mathbf{p} + \mathbf{p}^2 - M_N E - i\varepsilon} \\
&+ \int \frac{d^3 q}{(2\pi)^3} \Delta_d \left(E - \frac{\mathbf{q}^2}{2M_N}, \mathbf{q} \right) \cdot (i\mathcal{T}_s^{a,ik})_{\alpha a}^{\gamma c}(E; \mathbf{k}, \mathbf{q}) \\
&\quad \times \frac{M_N y_d^2}{2} \frac{(\sigma^j \sigma^k)_\gamma^\beta \delta_c^b}{\mathbf{q}^2 + \mathbf{q} \cdot \mathbf{p} + \mathbf{p}^2 - M_N E - i\varepsilon} \quad (\text{A6a}) \\
&+ \int \frac{d^3 q}{(2\pi)^3} \Delta_t \left(E - \frac{\mathbf{q}^2}{2M_N}, \mathbf{q} \right) \cdot (i\mathcal{T}_s^{b,iC})_{\alpha a}^{\gamma c}(E; \mathbf{k}, \mathbf{q}) \\
&\quad \times \frac{M_N y_d y_t}{2} \frac{(\sigma^j)_\gamma^\beta (\tau^C)_c^b}{\mathbf{q}^2 + \mathbf{q} \cdot \mathbf{p} + \mathbf{p}^2 - M_N E - i\varepsilon}
\end{aligned}$$

$$\begin{aligned}
(i\mathcal{T}_s^{b,iB})_{\alpha a}^{\beta b}(E; \mathbf{k}, \mathbf{p}) &= -\frac{iM_N y_d y_t}{2} \cdot (\sigma^i)_\alpha^\beta (\tau^B)_a^b \cdot \frac{1}{\mathbf{k}^2 + \mathbf{k} \cdot \mathbf{p} + \mathbf{p}^2 - M_N E - i\epsilon} \\
&+ \int \frac{d^3 q}{(2\pi)^3} \Delta_d \left(E - \frac{\mathbf{q}^2}{2M_N}, \mathbf{q} \right) \cdot (i\mathcal{T}_s^{a,ik})_{\alpha a}^{\gamma c}(E; \mathbf{k}, \mathbf{q}) \\
&\quad \times \frac{M_N y_d y_t}{2} \frac{(\sigma^k)_\gamma^\beta (\tau^B)_c^b}{\mathbf{q}^2 + \mathbf{q} \cdot \mathbf{p} + \mathbf{p}^2 - M_N E - i\epsilon} \quad (\text{A6b}) \\
&+ \int \frac{d^3 q}{(2\pi)^3} \Delta_t \left(E - \frac{\mathbf{q}^2}{2M_N}, \mathbf{q} \right) \cdot (i\mathcal{T}_s^{b,iC})_{\alpha a}^{\gamma c}(E; \mathbf{k}, \mathbf{q}) \\
&\quad \times \frac{M_N y_t^2}{2} \frac{\delta_\gamma^\beta (\tau^B \tau^C)_c^b}{\mathbf{q}^2 + \mathbf{q} \cdot \mathbf{p} + \mathbf{p}^2 - M_N E - i\epsilon}
\end{aligned}$$

for the coupled-channel n - d equation shown in Fig. 7, and analogously we have

$$\begin{aligned}
(i\mathcal{T}_{\text{full}}^{a,ij})_{\alpha a}^{\beta b}(E; \mathbf{k}, \mathbf{p}) &= -\frac{iM_N y_d^2}{2} \cdot (\sigma^j \sigma^i)_\alpha^\beta \delta_a^b \cdot \frac{1}{\mathbf{k}^2 + \mathbf{k} \cdot \mathbf{p} + \mathbf{p}^2 - M_N E - i\epsilon} \\
&- i\alpha M_N^2 y_d^2 \cdot \delta^{ij} \delta_\alpha^\beta \left(\frac{\mathbf{1} + \tau_3}{2} \right)_a^b \left[\frac{\mathcal{I}_{\text{bubble}}(E; \mathbf{k}, \mathbf{p})}{(\mathbf{k} - \mathbf{p})^2 + \lambda^2} - \frac{\rho_d}{2} \frac{1}{(\mathbf{k} - \mathbf{p})^2 + \lambda^2} \right] \\
&+ \int \frac{d^3 q}{(2\pi)^3} \Delta_d \left(E - \frac{\mathbf{q}^2}{2M_N}, \mathbf{q} \right) \cdot (i\mathcal{T}_{\text{full}}^{a,ik})_{\alpha a}^{\gamma c}(E; \mathbf{k}, \mathbf{q}) \cdot \left\{ \frac{M_N y_d^2}{2} \frac{(\sigma^j \sigma^k)_\gamma^\beta \delta_c^b}{\mathbf{q}^2 + \mathbf{q} \cdot \mathbf{p} + \mathbf{p}^2 - M_N E - i\epsilon} \right. \\
&\quad \left. + \alpha M_N^2 y_d^2 \cdot \delta^{kj} \delta_\gamma^\beta \left(\frac{\mathbf{1} + \tau_3}{2} \right)_c^b \left[\frac{\mathcal{I}_{\text{bubble}}(E; \mathbf{q}, \mathbf{p})}{(\mathbf{q} - \mathbf{p})^2 + \lambda^2} - \frac{\rho_d}{2} \frac{1}{(\mathbf{q} - \mathbf{p})^2 + \lambda^2} \right] \right\} \\
&+ \int \frac{d^3 q}{(2\pi)^3} \Delta_t \left(E - \frac{\mathbf{q}^2}{2M_N}, \mathbf{q} \right) \cdot (i\mathcal{T}_{\text{full}}^{b,iC})_{\alpha a}^{\gamma c}(E; \mathbf{k}, \mathbf{q}) \cdot \frac{M_N y_d y_t}{2} \cdot \frac{(\sigma^j)_\gamma^\beta (\tau^C)_c^b}{\mathbf{q}^2 + \mathbf{q} \cdot \mathbf{p} + \mathbf{p}^2 - M_N E - i\epsilon} \quad (\text{A7a})
\end{aligned}$$

$$\begin{aligned}
(i\mathcal{T}_{\text{full}}^{b,iB})_{\alpha a}^{\beta b}(E; \mathbf{k}, \mathbf{p}) &= -\frac{iM_N y_d y_t}{2} \cdot (\sigma^i)_\alpha^\beta (\tau^B)_a^b \cdot \frac{1}{\mathbf{k}^2 + \mathbf{k} \cdot \mathbf{p} + \mathbf{p}^2 - M_N E - i\epsilon} \\
&+ \int \frac{d^3 q}{(2\pi)^3} \Delta_d \left(E - \frac{\mathbf{q}^2}{2M_N}, \mathbf{q} \right) \cdot (i\mathcal{T}_{\text{full}}^{a,ik})_{\alpha a}^{\gamma c}(E; \mathbf{k}, \mathbf{q}) \cdot \frac{M_N y_d y_t}{2} \frac{(\sigma^k)_\gamma^\beta (\tau^B)_c^b}{\mathbf{q}^2 + \mathbf{q} \cdot \mathbf{p} + \mathbf{p}^2 - M_N E - i\epsilon} \\
&+ \int \frac{d^3 q}{(2\pi)^3} \Delta_t \left(E - \frac{\mathbf{q}^2}{2M_N}, \mathbf{q} \right) \cdot (i\mathcal{T}_{\text{full}}^{b,iC})_{\alpha a}^{\gamma c}(E; \mathbf{k}, \mathbf{q}) \cdot \left\{ \frac{M_N y_t^2}{2} \frac{\delta_\gamma^\beta (\tau^B \tau^C)_c^b}{\mathbf{q}^2 + \mathbf{q} \cdot \mathbf{p} + \mathbf{p}^2 - M_N E - i\epsilon} \right. \\
&\quad \left. + \alpha M_N^2 y_t^2 \cdot \delta_\gamma^\beta (\delta^{CB} - i\epsilon^{3CB}) \left(\frac{\mathbf{1} + \tau_3}{2} \right)_c^b \left[\frac{\mathcal{I}_{\text{bubble}}(E; \mathbf{q}, \mathbf{p})}{(\mathbf{q} - \mathbf{p})^2 + \lambda^2} - \frac{\rho_d}{2} \frac{1}{(\mathbf{q} - \mathbf{p})^2 + \lambda^2} \right] \right\} \quad (\text{A7b})
\end{aligned}$$

for the p - d equation depicted in Fig. 8.

Appendix B: Normalisation of the trinucleon wave functions

In this section we will give a brief derivation of the normalisation condition (39) for the triton wave functions used in Sec. V. In order to do that we need to introduce a little more formalism. For simplicity, we work with a simplified nucleon-deuteron system, where the

virtual spin-singlet state is neglected. The discussion could easily be carried out for the full coupled-channel system, but that would only complicate the notation.

Bethe–Salpeter equation

We start by considering the full two-body nucleon–deuteron propagator (Green’s function) G , which fulfils the (inhomogeneous) Bethe–Salpeter equation² in momentum space:

$$G(k, p; P) = G_0(k, p; P) + \int \frac{d^4q}{(2\pi)^4} \int \frac{d^4q'}{(2\pi)^4} G(k, q; P) \cdot K(q, q'; P) \cdot G_0(q', p; P). \quad (\text{B1})$$

G_0 is essentially a product of a nucleon propagator Δ_N and a deuteron propagator Δ_d . More precisely, we have

$$G_0(k, p; P) = (2\pi)^4 \delta^{(4)}(k - p) \cdot \Delta_d(\eta_d P + p) \cdot \Delta_N(\eta_N P - p), \quad (\text{B2})$$

where P is the total four-momentum of the system and $\eta_d + \eta_N = 1$. K represents the (doublet-projected) one-nucleon exchange diagram,

$$K(k_0, \mathbf{k}, p_0, \mathbf{p}; E) = \frac{-iy_d^2/2}{\eta_d E - \eta_N E + k_0 + p_0 - \frac{(\mathbf{k} + \mathbf{p})^2}{2M_N} + i\epsilon}, \quad (\text{B3})$$

as shown, for example, in Fig. 4.

Assuming the existence of a trinucleon bound state (the triton in our current toy model) at an energy $E = -E_B < 0$, one can show that

$$G(k, p; P) = i \frac{\psi_{B\mathbf{P}}(p) \psi_{B\mathbf{P}}^\dagger(k)}{E + E_B + i\epsilon} + \text{terms regular at } P_0 = E = -E_B, \quad (\text{B4})$$

i.e. G factorises at the bound state pole.

Three-dimensional reduction

We now consider a bound state at rest, *i.e.* $P = (-E_B, \mathbf{0})$, and define the *amputated* wave function

$$\mathcal{B}(p_0, \mathbf{p}) = \psi_{B\mathbf{0}}(p_0, \mathbf{p}) \cdot [\Delta_d(-\eta_d E_B + p_0, \mathbf{p})]^{-1} \cdot [\Delta_N(-\eta_N E_B - p_0, \mathbf{p})]^{-1}, \quad (\text{B5})$$

which fulfils the homogeneous equation

$$\mathcal{B}(p_0, \mathbf{p}) = \int \frac{d^4q}{(2\pi)^4} K(q, p; -E_B) \cdot \Delta_d(-\eta_d E_B + q_0, \mathbf{q}) \cdot \Delta_N(-\eta_N E_B - q_0, \mathbf{q}) \cdot \mathcal{B}(q_0, \mathbf{q}). \quad (\text{B6})$$

² For a discussion of the Bethe–Salpeter we refer to [39], which served as a starting point for our considerations.

Carrying out the dq_0 -integration picks up the residue from the nucleon propagator pole at $q_0 = -\eta_N E_B - \mathbf{q}^2/(2M_N) + i\epsilon$. From the resulting right hand side of (B6) we then find that

$$\mathcal{B}(\mathbf{p}) \equiv \mathcal{B}\left(-\eta_N E_B - \frac{\mathbf{p}^2}{2M_N}, \mathbf{p}\right) \quad (\text{B7})$$

fulfils the equation

$$\mathcal{B}(\mathbf{p}) = \int \frac{d^3q}{(2\pi)^3} K\left(\eta_N E - \frac{\mathbf{q}^2}{2M_N}, \mathbf{k}, \eta_N E - \frac{\mathbf{p}^2}{2M_N}, \mathbf{p}; E\right) \cdot \Delta_d\left(-E_B - \frac{\mathbf{q}^2}{2M_N}, \mathbf{q}\right) \cdot \mathcal{B}(\mathbf{q}). \quad (\text{B8})$$

This is essentially the single-channel equivalent of (36) (before S-wave projection), so we have established the connection of our current formalism to the triton wave functions $\vec{\mathcal{B}}_s$ in Sec. V. Note furthermore that

$$\phi(\mathbf{p}) \equiv \int \frac{dp_0}{2\pi} \psi(p_0, \mathbf{p}) = \Delta_d\left(-E_B - \frac{\mathbf{p}^2}{2M_N}, \mathbf{p}\right) \cdot \mathcal{B}(\mathbf{p}) \quad (\text{B9})$$

is a Schrödinger wave function. We now write (B1) in an operator notation as

$$G = G_0 + GK G_0 = G_0 + G_0 K G. \quad (\text{B10})$$

Defining

$$\tilde{G}(\mathbf{k}, \mathbf{p}; -E_B) = \int \frac{dk_0}{2\pi} \int \frac{dp_0}{2\pi} G(k, p; P), \quad (\text{B11})$$

we find

$$\tilde{G} \sim i \frac{|\phi\rangle \langle\phi|}{E + E_B} \quad \text{for } E \rightarrow -E_B, \quad (\text{B12})$$

where $|\phi\rangle$ corresponds to the wave function given in (B9), and

$$\tilde{G} = \tilde{G}_0 + \widetilde{G_0 K G}. \quad (\text{B13})$$

From this we readily derive the normalisation condition

$$i \langle\phi| \frac{d}{dE} \left(\tilde{G}_0^{-1} - \tilde{V} \right) |\phi\rangle \Big|_{E=-E_B} = 1, \quad (\text{B14})$$

where

$$\tilde{V} \equiv \tilde{G}_0^{-1} - \tilde{G}^{-1}. \quad (\text{B15})$$

A straightforward calculation shows that

$$\tilde{G}_0^{-1}(\mathbf{k}, \mathbf{p}; E) = (2\pi)^3 \delta^{(3)}(\mathbf{k} - \mathbf{p}) \cdot \left[\Delta_d\left(E - \frac{\mathbf{p}^2}{2M_N}, \mathbf{p}\right) \right]^{-1}, \quad (\text{B16})$$

and we also see that $|\mathcal{B}\rangle = \tilde{G}_0^{-1} |\phi\rangle$. The expression for \tilde{V} *a priori* looks more complicated, but one finds that in the formal expansion

$$\tilde{V} = \tilde{G}_0^{-1} - \left[\sum_{n=0}^{\infty} \left(-\tilde{G}_0^{-1} \widetilde{G_0 K G} \right)^n \right] \tilde{G}_0^{-1} \quad (\text{B17})$$

everything but the term

$$\widetilde{V}_1 \equiv \widetilde{G}_0^{-1} \widetilde{G}_0 \widetilde{K} \widetilde{G}_0 \widetilde{G}_0^{-1} \quad (\text{B18})$$

drops out, and we have

$$\widetilde{V}_1(\mathbf{k}, \mathbf{p}; E) = K \left(\eta_N E - \frac{\mathbf{k}^2}{2M_N}, \mathbf{k}, \eta_N E - \frac{\mathbf{p}^2}{2M_N}, \mathbf{p}; E \right). \quad (\text{B19})$$

The essential ingredient to see this is

$$\cdots \widetilde{G}_0 \widetilde{G}_0^{-1} \widetilde{G}_0 \cdots = \cdots \widetilde{G}_0 \cdots, \quad (\text{B20})$$

which, in turn, follows from the fact that the nucleon propagator residues are always picked up in such a way that one deuteron propagator is cancelled by the inverse propagator in \widetilde{G}_0^{-1} , *cf.* Eq. (B16). Altogether, we have shown that (B14) is just the single-channel version of the normalisation condition (39) stated in Sec. V (modulo S-wave projection), where the functions $I_{d,t}$ correspond to \widetilde{G}_0^{-1} .

-
- [1] S. R. Beane, W. Detmold, K. Orginos and M. J. Savage, *Prog. Part. Nucl. Phys.* **66** (2011) 1 [arXiv:1004.2935 [hep-lat]].
 - [2] S. R. Beane, P. F. Bedaque, W. C. Haxton, D. R. Phillips and M. J. Savage, arXiv:nucl-th/0008064.
 - [3] P. F. Bedaque and U. van Kolck, *Ann. Rev. Nucl. Part. Sci.* **52** (2002) 339 [arXiv:nucl-th/0203055].
 - [4] E. Epelbaum, H.-W. Hammer and U.-G. Meißner, *Rev. Mod. Phys.* **81** (2009) 1773 [arXiv:0811.1338 [nucl-th]].
 - [5] D. B. Kaplan, M. J. Savage and M. B. Wise, *Nucl. Phys. B* **534**, (1998) 329 [arXiv:nucl-th/9802075].
 - [6] U. van Kolck, *Nucl. Phys. A* **645**, (1999) 273 [arXiv:nucl-th/9808007].
 - [7] H. A. Bethe, *Phys. Rev.* **76** (1949) 38.
 - [8] V. Efimov, *Nucl. Phys. A* **362** (1981) 45.
 - [9] H.-W. Hammer and L. Platter, *Ann. Rev. Nucl. Part. Sci.* **60** (2010) 207 [arXiv:1001.1981 [nucl-th]].
 - [10] X. Kong and F. Ravndal, *Phys. Lett. B* **450** (1999) 320 [arXiv:nucl-th/9811076].
 - [11] X. Kong and F. Ravndal, *Nucl. Phys. A* **665** (2000) 137 [arXiv:hep-ph/9903523].
 - [12] S.-I. Ando, J. W. Shin, C. H. Hyun and S. W. Hong, *Phys. Rev. C* **76** (2007) 064001 [arXiv:0704.2312 [nucl-th]].
 - [13] T. Barford and M. C. Birse, *Phys. Rev. C* **67** (2003) 064006 [arXiv:hep-ph/0206146].
 - [14] S.-I. Ando and M. C. Birse, *Phys. Rev. C* **78** (2008) 024004 [arXiv:0805.3655 [nucl-th]].
 - [15] X. Kong and F. Ravndal, *Phys. Rev. C* **64** (2001) 044002 [arXiv:nucl-th/0004038].
 - [16] S.-I. Ando, J. W. Shin, C. H. Hyun, S. W. Hong and K. Kubodera, *Phys. Lett. B* **668** (2008) 187 [arXiv:0801.4330 [nucl-th]].
 - [17] V. Efimov, *Phys. Lett. B* **33** (1970) 563.
 - [18] C. A. Bertulani, H.-W. Hammer and U. van Kolck, *Nucl. Phys. A* **712** (2002) 37 [arXiv:nucl-th/0205063].

- [19] G. Rupak and X. Kong, Nucl. Phys. A **717** (2003) 73 [arXiv:nucl-th/0108059].
- [20] S. Ando and M. C. Birse, J. Phys. G: Nucl. Part. Phys. **37** (2010) 105108 [arXiv:1003.4383 [nucl-th]].
- [21] J. Kirscher, H. W. Griesshammer, D. Shukla and H. M. Hofmann, Eur. Phys. J. A **44** (2010) 239 [arXiv:0903.5538 [nucl-th]].
- [22] P. F. Bedaque, H.-W. Hammer and U. van Kolck, Nucl. Phys. A **676** (2000) 357 [arXiv:nucl-th/9906032].
- [23] P. F. Bedaque, G. Rupak, H. W. Griesshammer and H.-W. Hammer, Nucl. Phys. A **714** (2003) 589 [arXiv:nucl-th/0207034].
- [24] E. Braaten and H.-W. Hammer, Phys. Rept. **428** (2006) 259 [arXiv:cond-mat/0410417].
- [25] F. Gabbiani, P. F. Bedaque and H. W. Griesshammer, Nucl. Phys. A **675** (2000) 601 [arXiv:nucl-th/9911034].
- [26] D. R. Phillips and T. D. Cohen, Phys. Lett. B **390** (1997) 7 [arXiv:nucl-th/9607048].
- [27] J. D. Jackson and J. M. Blatt, Rev. Mod. Phys. **22** (1950) 77.
- [28] D. R. Harrington, Phys. Rev. **139** (1965) B691.
- [29] H. W. Griesshammer, Nucl. Phys. A **760** (2005) 110 [arXiv:nucl-th/0502039].
- [30] L. Platter, D. R. Phillips, Few Body Syst. **40** (2006) 35 [arXiv:cond-mat/0604255].
- [31] C. Ji, D. R. Phillips, L. Platter, Europhys. Lett. **92** (2010) 13003 [arXiv:1005.1990 [cond-mat.quant-gas]].
- [32] C. van der Leun and C. Anderliesten, Nucl. Phys. A **380** (1982), 261.
- [33] J. J. de Swart, C. P. F. Terheggen and V. G. J. Stoks, arXiv:nucl-th/9509032.
- [34] J. R. Bergervoet, P. C. van Campen, W. A. van der Sanden and J. J. de Swart, Phys. Rev. C **38** (1988) 15.
- [35] J. Arvieux, Nucl. Phys. A **221** (1973) 253.
- [36] R. S. Christian and J. L. Gammel, Phys. Rev. **91** (1953) 100.
- [37] L. Platter, Phys. Rev. C **74** (2006) 037001 [arXiv:nucl-th/0606006].
- [38] R. A. Brandenburg, S. A. Coon, and P. U. Sauer, Nucl. Phys. A **294** (1978) 395.
- [39] D. Lurie, *Particles and Fields*, Interscience Publishers (1968).